Available online at www.sciencedirect.com
ScienceDirect
Polymer 49 (2008) 1841–1852
polymer
www.elsevier.com/locate/polymer

Quantification of the layer dispersion degree in polymer layered silicate nanocomposites by transmission electron microscopy

Z.P. Luo [a,*], J.H. Koo [b]

[a] Microscopy and Imaging Center, Biological Sciences Building West, Texas A&M University, College Station, TX 77843-2257, USA
[b] Department of Mechanical Engineering, The University of Texas at Austin, Austin, TX 78712-0292, USA

Received 23 January 2008; accepted 16 February 2008
Available online 21 February 2008

Abstract

As the performance of polymer layered silicate nanocomposites strongly depends on their interior layer dispersion, quantification of the layer dispersion degree is needed. In this work, a new methodology was developed to determine the dispersion parameter $D_{0.1}$, based on the measurement of the free-path spacing distance between the single clay sheets from the transmission electron microscopy (TEM) images. Several examples of exfoliated, intercalated, and immiscible composites were studied. It was found that the exfoliated composites had $D_{0.1}$ over 8%, while that of intercalated composites were between 4 and 8%. In the case of intercalation, a high frequency peak appeared at a short spacing distance in the histogram, which was a characteristic of the intercalation, distinct from the exfoliation. The main utility of this TEM methodology is for the quantification of exfoliated or intercalated samples with small number of layers with stacks. The dispersion parameter $D_{0.1}$ below 4% was suggested to classify as immiscible. A unique advantage of the TEM measurement is that the dispersion degree of different fillers can be counted individually.

Keywords: Dispersion quantification; Polymer/clay composite materials; Transmission electron microscopy (TEM)

1. Introduction

The layered silicate minerals, clay, with layered structures, have been used in polymer composites for a quite long time, more than half a century ago [1]. Their structures are characterized by two tetrahedral coordinated silicon layers fused to a central octahedrally coordinated metal (Al^{3+} or Mg^{2+}) layer. The entity of the three sandwiched layers, with 1 nm thickness and few hundred nanometers size in other two dimensions, is stacked together with a regular van der Waals gap, the so-called gallery [2]. Depending on the clay platelet opening degree after integration with polymer matrix, the composites are roughly classified as [3]: (1) exfoliated or delaminated – layers are fully open; (2) intercalated – layers partially open; and (3) immiscible – layers remain closed (tactoid). There exists layer ordering, or a status between them, or even a mixture of these classifications, which in the last two cases make the classification undistinguishable. Because of the high aspect ratio of the clay platelet, the silicate clay has huge potential to increase the clay/polymer interfacial areas to enhance their properties, if the layers are fully open to let the polymer enter the galleries. Therefore, opening the layers has been one of the major goals in developing the polymer layered silicate nanocomposites (PLSNs), as the PLSNs with exfoliated fillers exhibit extraordinary mechanical and physical properties [4–8]. In order to overcome the interlayer van der Waals bonding barrier to achieve the layer exfoliation, two major approaches have been developed, i.e. *in situ* intercalative polymerization [4,9–14] and melt intercalation [15–20]. The former process involves the dispersion of the clay filler into the monomers followed by polymerization, and in the latter one, the clay filler is mixed into the molten polymer.

It is known that the clay layer exfoliation degree within the matrix is a function of the composite processing parameters [21,22]. In order to correlate the material microstructure

* Corresponding author. Tel.: +1 979 845 1129; fax: +1 979 847 8933
E-mail address: luo@mic.tamu.edu (Z.P. Luo).

0032-3861/$ - see front matter © 2008 Elsevier Ltd. All rights reserved.
doi:10.1016/j.polymer.2008.02.028

with their processing and properties, it is essential to quantify the clay platelets' dispersion degree. Currently, the following methods have been used to evaluate the clay dispersion: (1) transmission electron microscopy (TEM) [3,23–30], (2) X-ray diffraction (XRD) [3,23,24,28], (3) solid-state nuclear magnetic resonance (NMR) [31,32], (4) rheological techniques [33], and (5) atomic force microscopy (AFM) [34,35]. The TEM method, with resolution typically around several angstroms, provides a direct observation of the layer dispersion [3,23–30]. By taking the advantage of the layered structure characteristic, on the other hand, the XRD monitors the layer opening degrees of PLSNs [3,23,24,28] from the measurement of the basal layer spacing d_{001} as compared to the original one d_0, i.e. immiscible when $d_{001} = d_0$, intercalated when $d_{001} > d_0$, and exfoliated when no peak appears by the layer disordering. However, as discussed by Morgan and Gilman [3], in some cases the XRD method may confuse the immiscible or exfoliated status. The solid-state NMR [31] measures the polymer/clay interfacial areas and the layer spacing. A reference sample with supposedly fully exfoliated structure was needed to obtain a parameter ε that reflects the dispersion degree [31]. The rheological method [33] has been attempted to measure the rheological responses to reflect the clay dispersion, with the aid of additional TEM and XRD analyses [33]. The AFM has been applied to study the PLSNs [34,35], but its effectiveness needs large exploration. At present, the TEM and XRD are probably the two mostly used approaches. It should be mentioned that all of the XRD, NMR and rheological approaches measure the bulk sample average information in different ways. If a sample contains multi-fillers, it is impossible to use these methods to evaluate the dispersion of individual fillers. At this point, the TEM is especially powerful since different fillers can be identified.

So far, the TEM is mainly used as a tool to compare the layer dispersion visually. However, limited quantitative microscopy has also been made so far in different ways. Basically, these studies can be classified as the following methods:

(1) *Particle size measurement (PSM)*: Nam and co-workers [26] proposed to measure the clay particle length L_{clay} and thickness d_{clay} of dispersed clay stacks, and the correlation length ξ_{clay} between these stacks. These parameters were then used to estimate the average number of individual layers in a clay clump. Recently, Vermogen et al. [30] used this PSM method to study the clay exfoliation behavior, with an additional parameter, aspect ratio AR, of the stack. The higher the AR value, the lesser the number of layer platelets within the stack and thus higher dispersion degree. Certainly, the single clay platelet has the highest AR. They classified the clay stacks into six groups with different number of platelets involved, i.e. micron-size agglomerates, middle-size tactoids, 5–10 sheet tactoids, 3–5 sheet tactoids, 2–3 tactoids, and individual exfoliated sheet. Each group was characterized by the above parameters as compared to three different samples.

(2) *Particle density measurement (PDM)*: Dennis et al. [25] and Fornes et al. [27] measured the clay particle density, i.e. the number of aggregated particles over a certain area, to compare the dispersion degree of different samples. An entity of a stack is counted as a single clay particle. Therefore, a higher density indicates larger degree of the clay exfoliation, and thus higher dispersion degree.

(3) *Linear intercept distance measurement (LIDM)*: Eckel et al. [29] placed an array of parallel lines over the TEM micrographs, and then divided the total length of the lines by the number of times the lines intersect the clay particles to obtain the linear intercept distance, i.e. the average clay particle spacing along the lines. As a stack of sheets is counted as an entity, smaller linear intercept distance indicates more number of particles along the lines and thus a better dispersion. Similar distance measurement was also made between platelets recently [32].

In this work, we present a new methodology, named as free-path spacing measurement (FPSM), to quantify the layer dispersion degrees from the TEM images, based upon the stereological principles [36–40]. In the following section, this method will be given in detail, and then it will be applied to study the dispersion in different polymer systems, with exfoliated, intercalated and immiscible cases. A comparison of this method with previous ones will also be discussed.

2. Experimental section

The polymer matrices used in this study were polyester polycaprolactone (Pellethane 2102 series) 2102A, polyamide PA11 (or nylon 11), polyamide PA12 (or nylon 12), cyanate ester PT30 and PT15, and epoxy. The montmorillonite Cloisite 30B clay was supplied by Southern Clay Products, Gonzales, Texas. Its layer spacing (d_{001}), as determined by XRD, is 1.85 nm. The Exolit OP 1230 intumescent fire retardant (FR) additives, supplied by Clariant, were also used in addition to the 30B clay. The polymer composites were prepared by mechanical mixing of nanoparticles into the polymer matrices using either a well-established twin-screw extrusion process for thermoplastics and elastomers, or high shear mixing for thermosets. The TEM specimens, with thickness less than 100 nm, were prepared by an ultramicrotome with a diamond knife at 5–6° cutting angle, or by an ion mill with a cold stage. The latter method involved grinding, polishing, dimpling and finally ion milling with liquid N_2 cooling until perforation. In both cases, no sample staining was used. The TEM analysis was performed in a JEOL 2010 microscope at the working voltage of 200 kV (with wavelength $\lambda = 0.00251$ nm), with spherical aberration coefficient $C_s = 1$ mm. Its optimum defocus [41], Scherzer defocus, is $\Delta f_{Sch} = -((4/3)C_s\lambda)^{1/2} = -58$ nm, which gives a point resolution of $r_{Sch} = 0.66C_s^{1/4}\lambda^{3/4} = 0.23$ nm. To image the clay single platelets, images were taken at near the Scherzer defocus to achieve the highest resolution at high magnifications, typically above ×50,000. However, for immiscible samples with large tactoids, it would be very difficult to count the single layer spacing between the tactoids, and thus images were taken at much large defocus values, about $(5-15)\Delta f_{Sch}$, to image the clay clusters composed of a number

of clay platelets. These images of immiscible samples were taken at lower magnifications, typically below ×50,000, to accommodate more clay particles. For accurate distance measurement, all of the TEM imaging magnifications were calibrated using standards of 6*H*-SiC lattice fringes [42] and commercial cross-line grating replica.

A general methodology to measure the dispersion degree has been established by us recently [43]. To apply this methodology to the PLSN system, TEM is especially useful because of its high resolution dealing with the nanoclay reinforcements. As shown in Fig. 1(a) for a schematic microstructure of PLSNs, a random line is used to intercept the clay platelets to obtain free-path spacing data x_i, between the platelets. As the platelet thickness is thin (1 nm), the free-path distance can be roughed as the distance between platelets. Note that if the line intercepts with a stack of platelets, the distance between each platelet within this stack is measured to reflect the entire dispersion level (the appearance of stacks decreases the dispersion). If two platelets touch each other, the distance $x = 0$. Afterwards, a histogram of the spacing data is constructed, as shown in Fig. 1(b). The dispersion parameter, $D_{0.1}$, is defied as the probability of the free-path distance distribution in the range of $0.9-1.1\mu$ [43], where μ is the mean spacing. As $D_{0.1}$ is deduced from the free-path distance distribution, it is dimensionless and not related to the layer shape, size, aggregation or concentration. In this method, a higher $D_{0.1}$ value indicates more spacing data close to the mean μ, and thus a better dispersion level. The dispersion of 100% means all of the platelets are equally spaced, which is technically impossible in reality. Usually, the free-path distance distribution obeys a lognormal distribution model, in which case $D_{0.1}$ is formularized as [43]:

$$D_{0.1} = 1.1539 \times 10^{-2} + 7.5933 \times 10^{-2}(\mu/\sigma) + 6.6838 \times 10^{-4}(\mu/\sigma)^2 - 1.9169 \times 10^{-4}(\mu/\sigma)^3 + 3.9201 \times 10^{-6}(\mu/\sigma)^4 \quad (1)$$

Here, σ is the standard deviation.

An example TEM image is shown in Fig. 2. The followings are the detailed steps to apply this method to quantify the dispersion degree $D_{0.1}$:

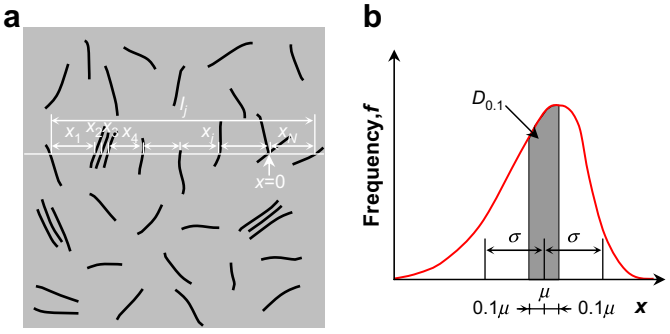

Fig. 1. (a) Schematic microstructure of clay platelets (in dark color) composite, where a random line is used to intercept the platelets to get spacing measurements; (b) clay layer free-path spacing histogram, with the dispersion parameter $D_{0.1}$ defined from the frequency function $f(x)$.

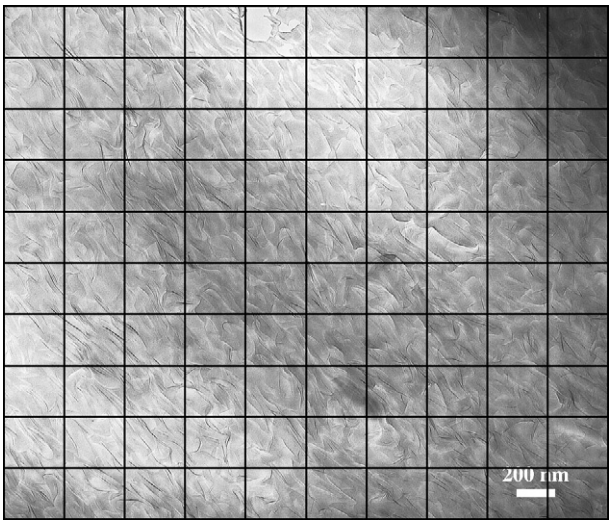

Fig. 2. An example of a TEM image, which is divided by 10 × 10 grid lines for the dispersion quantification along the grid lines.

(1) Place arrays of parallel lines over the TEM micrograph. For isotropic sample, two perpendicular arrays are applied so that dispersions can be measured along both directions. If the sample is anisotropic, the array of parallel lines can be placed along any particular directions so that the dispersion $D_{0.1}$ is measured along that direction. Depending on the sampling number N of measurements which should be over 100, a TEM image is normally divided into 10–20 grid lines. If the TEM image is taken randomly (or after rotation randomly), the grid lines are placed horizontally and vertically to make the distance measurement easier;
(2) Measure the free-path distance x_i, the distance of the matrix, between the clay sheets, along the intercept lines as shown in Fig. 1(a). In this work, a freeware *ImageJ* [44] program was used for the measurement. Note that scale bars on the TEM negatives could produce up to 10% error, thus the scale bars need calibration for accurate distance measurement. The sampling number N is expected to be greater than 100; otherwise increase the grid lines, or use more micrographs even make montages of the micrographs to achieve more measurements;
(3) Based on a set of free-path distance data, calculate the data sample mean $\bar{x} = \sum_i x_i/N$ and data sample standard deviation $s = \sqrt{\sum_i (x_i - \bar{x})^2/(N-1)}$;
(4) Calculate the dispersion quantity $D_{0.1}$ by using the ratio $\bar{x}/s$ to substitute μ/σ in Eq. (1). For the details to plot histogram and the lognormal curve fitting, see Ref. [43].

The accuracy of the $D_{0.1}$ measurement strongly depends on the sampling. The TEM image must be representative and in an appropriate magnification so that the single clay sheets are resolved while maintaining a wide range of view to accommodate more clay platelets for the measurement. For accurate comparison of $D_{0.1}$ of different samples, at least three representative TEM images are needed for the quantification. In case the sample microstructure is not uniform, even more representative TEM images should be used for averaging.

3. Results

In this work, we studied the dispersion of 30B clay into six different systems (2102A, PA11, PA12, PT30, PT15, and epoxy) at different loading levels from 1 to 10 wt%, as listed in Table 1. The 1230 FR particles were also added with 30B into the PA11 matrix to examine the interaction of the FR particles with the 30B clay. Quantitative measurements based on the TEM images are made on these samples, and the measured results of mean layer spacing $\bar{x}$, standard deviation s, and their ratio $\bar{x}/s$ are listed in Table 1. The dispersion parameter $D_{0.1}$ is calculated by using $\bar{x}/s$ to estimate μ/σ in Eq. (1). It is found that samples of 2102A, PA11 (including the addition of 1230 FR particles), and PA12 have good dispersions at all loading levels of 30B. In these samples, the original large 30B clay tactoids are broken up and well dispersed all over the samples, although both exfoliated and intercalated types are identified. The PT30 samples have lower dispersion level, but they are still classified as the intercalated type, as will be shown later. However, in the PT15 and epoxy samples, large clumps are found, so they are classified as the immiscible type. Typical examples of exfoliated, intercalated and immiscible samples are given in the following sections.

3.1. Exfoliated dispersion

A typical microstructure of 2102A with 7.5 wt% 30B clay is shown in Fig. 3(a). Generally, the original big clay clumps are completely broken up and the clay platelets dispersed all over the entire area. The framed area is magnified Fig. 3(b), where it is seen that the clay platelets are exfoliated and well dispersed within the matrix. For quantitative measurements, Fig. 3(a) is divided by 10 × 10 grid lines, and the free-path spacing distance between the clay platelets along these grid lines are measured to construct a histogram, as shown in (c). A lognormal distribution [43] curve is superimposed, which fits the measured frequency curve. Therefore, the dispersion is calculated using Eq. (1) for the lognormal distribution model. Instead, a normal distribution only gives symmetrical curve beside the peak position. The statistics of the measurements are labeled in Fig. 3(c). The mean

Table 1
Results of quantitative measurements

Matrix	Loading level (wt%)	Mean free-path spacing, $\bar{x}$ (nm)	Standard deviation, s (nm)	$\bar{x}/s$	$D_{0.1}$ (%)	Classification
2102A	2.5	105.1	110.6	0.9503	8.4	Exfoliated
	5.0	66.3	68.0	0.9750	8.6	Exfoliated
	7.5	45.0	39.9	1.1278	9.8	Exfoliated
	10.0	27.8	33.4	0.8323	7.5	Intercalated
PA11	2.5	109.7	139.7	0.7853	7.2	Intercalated
	5.0	55.8	71.9	0.7761	7.1	Intercalated
	7.5	42.9	39.9	1.0752	9.4	Exfoliated
	10.0	28.6	25.6	1.1172	9.7	Exfoliated
PA12	2.5	115.0	151.8	0.7576	6.9	Intercalated
	5.0	62.5	64.9	0.9630	8.5	Exfoliated
	7.5	44.9	45.2	0.9934	8.7	Exfoliated
PT30	2.5	107.5	273.4	0.3932	4.2	Intercalated
	3.5	80.0	171.7	0.4659	4.7	Intercalated
PT15	5.0	317.5[a]	1069.1[a]	0.2970[a]	3.4[a]	Immiscible
Epoxy	1.0	991.1[a]	3651.8[a]	0.2714[a]	3.2[a]	Immiscible
	2.0	378.9[a]	539.6[a]	0.7022[a]	6.5[a]	Immiscible
	5.0	231.5[a]	357.8[a]	0.6470[a]	6.1[a]	Immiscible
	10.0	147.2[a]	267.5[a]	0.5503[a]	5.4[a]	Immiscible
PA11 + 1230	5.0	55.0	61.2	0.8987	8.0	Exfoliated/ Intercalated
	7.5	40.4	42.3	0.9551	8.5	Exfoliated

[a] Note: the measurements of the immiscible PT15 and epoxy are made based on the cluster measurement rather than single layer measurements.

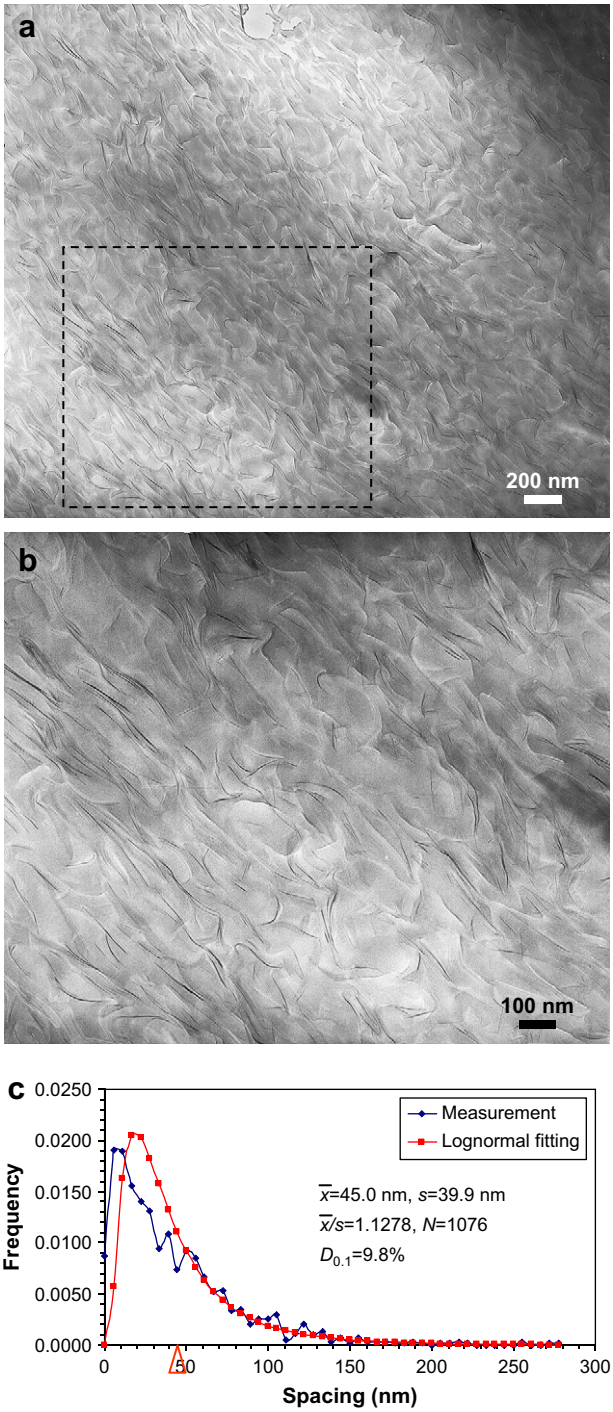

Fig. 3. (a) Microstructure of exfoliated 2102A with 7.5 wt% 30B; (b) magnified image from the framed area in (a); (c) layer spacing distance histogram. Curve fitting by lognormal distribution is superimposed and the arrowhead indicates the mean spacing position.

spacing ($\bar{x}$) is 45.0 nm, with a standard deviation (s) of 39.9 nm, and thus $\bar{x}/s = 1.1278$, hence $D_{0.1} = 9.8\%$. Therefore, about 9.8% spacing data are in the range of 40.5–49.5 nm that corresponds to the range of $0.9 - 1.1\bar{x}$. The mean spacing of 45.0 nm is much longer than the original crystalline layer spacing of $d_{001} = 1.85$ nm, implying that good exfoliations of the single clay platelets are achieved in this sample.

Another example of exfoliated sample, PA11, with a higher loading of 10 wt% 30B clay, is shown in Fig. 4(a). The clay particles are seen as exfoliated, and the platelets are well dispersed over the entire area. Similar exfoliated microstructures were observed previously by Fornes and Paul [45], and Eckel and co-workers [29] by the nylon's polar nature. The entire area of Fig. 4(a) is divided by 10×10 grid lines along the horizontal and vertical directions, respectively, and then the spacing distance between the clay platelets along the grid lines are measured to establish the histogram as shown in (b). A lognormal distribution [43] curve is superimposed. As labeled in Fig. 4(b), the statistics of the measurements indicate that the mean spacing is 28.6 nm, with a standard deviation of 25.6 nm, and thus $\bar{x}/s = 0.1172$, which yields $D_{0.1} = 9.7\%$. This dispersion level is almost the same as the 2102A sample shown in Fig. 3, although they are at the different loading levels. It is noticed that the mean spacing of 28.6 nm is greatly shorter than 45.0 nm of the previous sample shown in Fig. 3, which is consistent with the loading raise from 7.5 to 10 wt%. If one uses the linear intercept distance between the clays to evaluate the dispersion, as previously studied [29,32], the intercept distance is not comparable between these two samples at different loadings. However, the dispersion level $D_{0.1}$ studied here is dimensionless which is independent of the loading level.

3.2. Intercalated dispersion

A typical microstructure of PA12 with a loading of 2.5 wt% 30B is shown in Fig. 5(a). The platelets are widely spaced because of the lower filler content. The original clay particles are broken up and the clay particles are well dispersed overall; while aggregations composed of few platelets exist, as shown in the enlargement in Fig. 5(b) from the central framed area of (a). Previously reported pictures also exhibited aggregations of few platelets [45,46]. Therefore, this sample demonstrates intercalation, instead of exfoliation, as for 2102A in Fig. 3 and PA11 in Fig. 4. In order to increase the measurement N, Fig. 5(a) is shown in a lower magnification and it is divided by 20×20 grid lines to construct the histogram in (c). It is seen from Fig. 5(c) that the spacing data cover a wide range. In the short spacing range, as shown in the magnified part in Fig. 5(d), a high frequency peak appears at 2.8 nm, which means these platelets within clumps are just slightly open. The appearance of this sharp peak in the short distance range is an evident indication of the intercalation. Although the peak position depends on the group number of the sampling to plot the histogram, it reflects the high frequency spacing data in a rough range. Even if the platelets remain at the original distance, the breaking up of the original large clumps and the dispersion of the smaller aggregates would be considered as intercalated. In the presence of clustering, as discussed previously [43], one may still calculate the dispersion using the entire range spacing data, but the dispersion degree is decreased by the clustering. The mean spacing is measured as 115.0 nm, with a standard deviation of 151.8 nm, and thus $\bar{x}/s = 0.7576$. Hence, this intercalated example has $D_{0.1} = 6.9\%$, which is lower than the exfoliated dispersions shown in Figs. 3 and 4 because of the existence of clusters with few platelets included.

Another example of intercalated case, PT30 with 3.5 wt% 30B, is shown in Fig. 6(a), where more platelets aggregate into clumps. An enlarged image is shown in Fig. 6(b). The image shown in Fig. 6(a) is divided by 20×20 grid lines to measure the spacing distance between the platelets, and the histogram is constructed as shown in (c), which is magnified to show the short spacing range (d). Similar to the case shown in Fig. 5(d), the histogram in Fig. 6(d) shows a sharp peak at

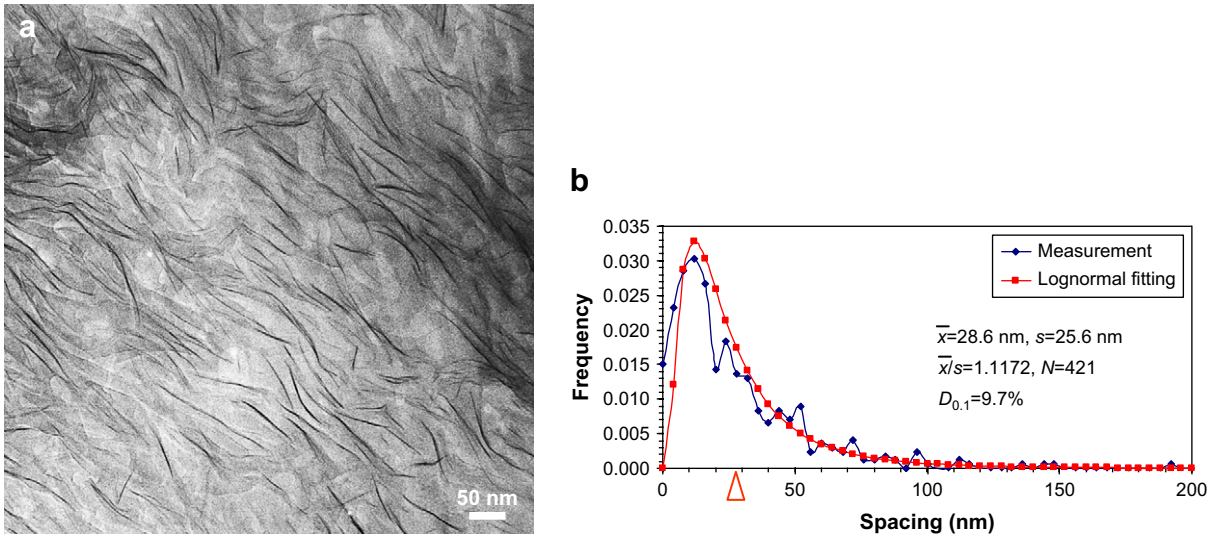

Fig. 4. (a) Microstructure of exfoliated PA11 with 10 wt% 30B; (b) layer spacing distance histogram. Curve fitting by lognormal distribution is superimposed and the arrowhead indicates the mean spacing position.

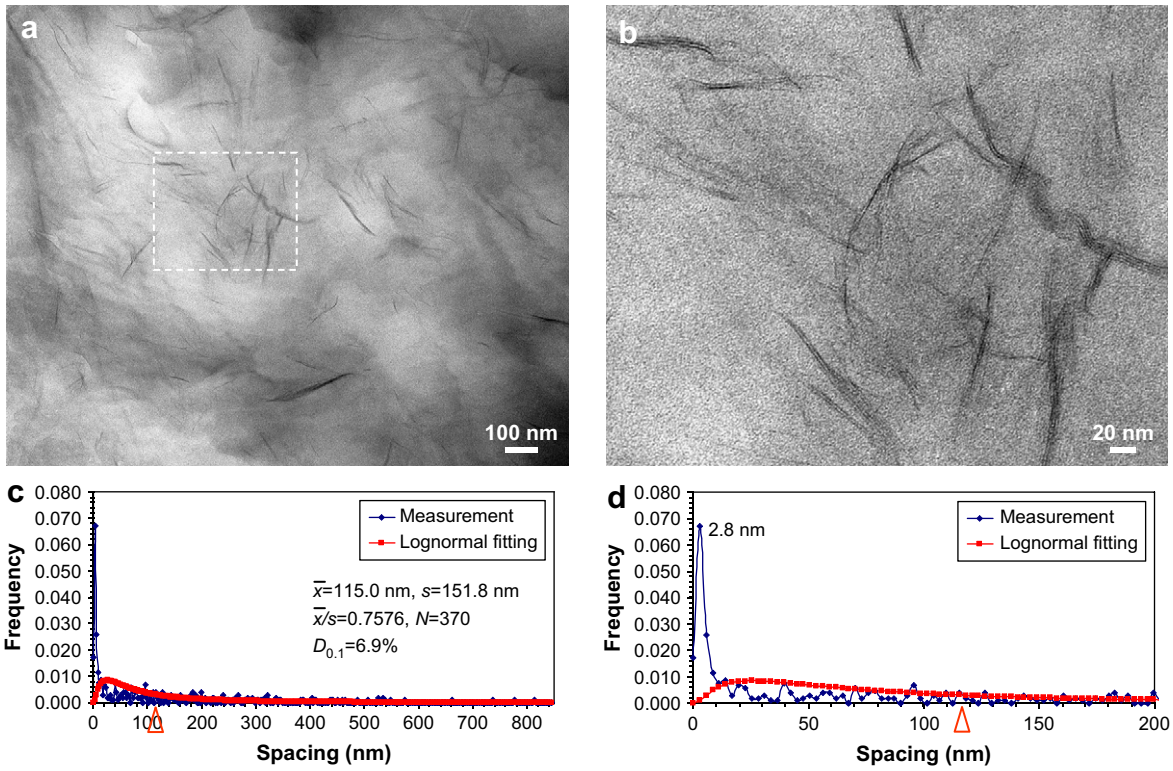

Fig. 5. (a) Microstructure of intercalated PA12 with 2.5 wt% 30B; (b) magnified image from the framed area in (a); (c) layer spacing distance histogram; (d) enlarged histogram from (c) showing the details in the short spacing range from 0 to 200 nm. The sharp high frequency peak at 2.8 nm in (d) is an indication of the intercalation. Curve fitting by lognormal distribution is superimposed and the arrowheads indicate the mean spacing position.

3.1 nm, indicating the presence of intercalation. The mean spacing is measured as 80.0 nm, with a standard deviation of 171.7 nm, and thus $\bar{x}/s = 0.4659$. Hence, the dispersion parameter $D_{0.1} = 4.7\%$, which is lower than the dispersion level of 6.9% in sample PA12 (Fig. 5), because of the fact of more platelets within a cluster. Considering the intercalated PT30 with 2.5 wt% 30B has even lower $D_{0.1} = 4.2\%$, it is suggested that dispersion level above 4% is classified as intercalated, and below it, immiscible because of sufficient number of platelets within a cluster.

3.3. Immiscible dispersion

For immiscible samples with large tactoids, it would be very difficult to count the single layer spacing in the same way for the above exfoliated/intercalated samples. In order to make this task easier, images are taken at larger defocus values to obtain cluster images. An example of the microstructure of PT15 with 5 wt% 30B clay is shown in Fig. 7(a), where isolated large clumps are seen. At this low magnification, a sheet seen is actually composed of a cluster of platelets if imaged at the Scherzer defocus, as shown in the magnified image in Fig. 7(b), from the framed area in (a). For simplicity, we count only the cluster sheets for the dispersion. Fig. 7(a) is then divided by 10×10 grid lines along the horizontal and vertical directions, respectively, and then the free-path spacing between the cluster sheets along the grid lines are measured to establish the histograms in (c). The spacing data scatter very largely, with a high frequency peak at 29.3 nm as shown in the short spacing range in Fig. 7(d). The mean cluster spacing is measured as 317.5 nm, with a large standard deviation of 1069.1 nm, and thus $\bar{x}/s = 0.2970$, hence $D_{0.1}^{\text{cluster}} = 3.4\%$. In fact, if one counts the single clay platelet spacing instead of the clusters, like those shown in Fig. 7(b), the dispersion is expected to be even lower because of the even larger data scattering for the single platelets.

Another immiscible example, the microstructure of epoxy with 2 wt% 30B with large clumps, is shown in Fig. 8(a) taken at larger defocus. As compared to Fig. 7, these clumps, with smaller size, distribute more evenly. This image is divided by 10×10 grid lines, and the spacing of the clusters is measured to construct the histogram in Fig. 8(b). The mean cluster spacing is measured as 378.9 nm, which is longer than 317.5 nm at the 5 wt% loading level shown in Fig. 7. The standard deviation is 539.6 nm, and thus $\bar{x}/s = 0.7022$, hence $D_{0.1}^{\text{cluster}} = 6.5\%$. The clusters in this sample have a better dispersion than those in the PT15 sample shown in Fig. 7.

3.4. Dispersion of different fillers

A unique advantage of the TEM measurement over others, by XRD, NMR, or rheological techniques, is that different fillers can be visually differentiated or chemically identified with the aid of advanced microanalysis techniques, such as mapping using X-ray energy-dispersive spectroscopy (EDS) or electron energy-loss spectroscopy (EELS). Therefore, their dispersions can be measured separately. Fig. 9(a) shows a microstructure of PA11 with 20 wt% 1230 FR particles plus

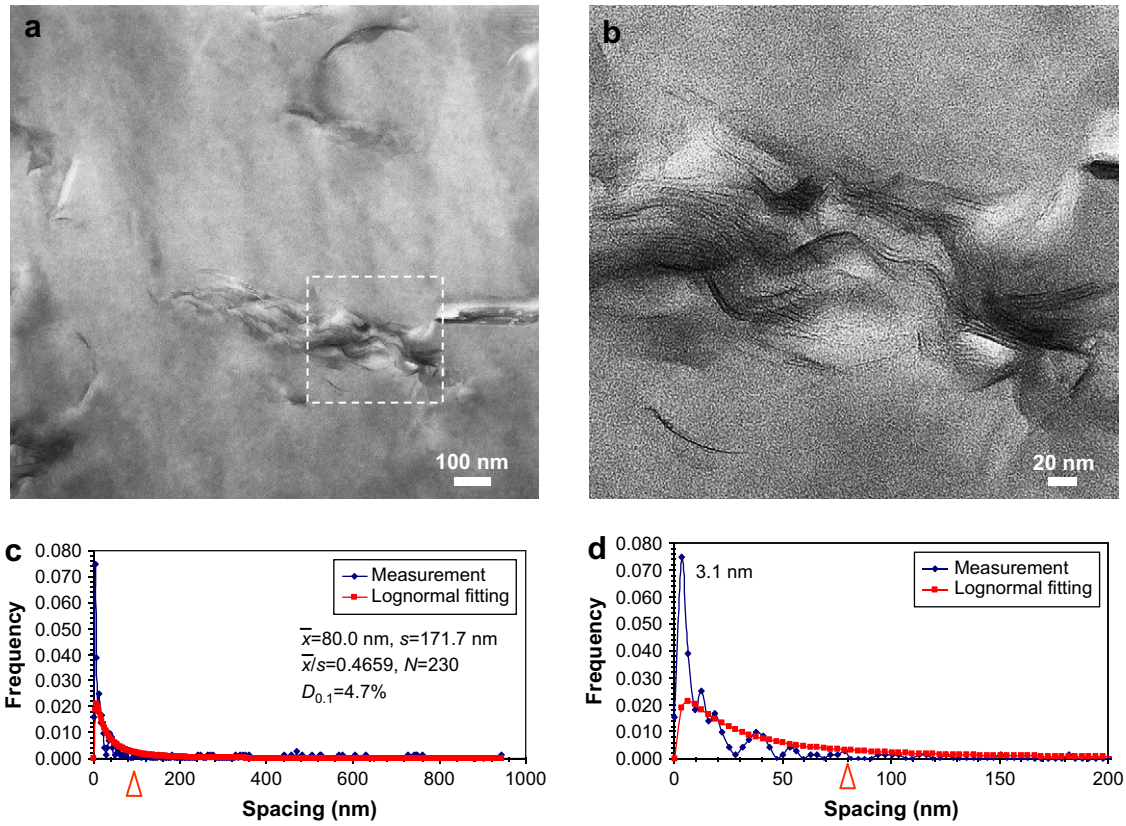

Fig. 6. (a) Microstructure of intercalated PT30 with 3.5 wt% 30B; (b) magnified image from the framed area in (a); (c) layer spacing distance histogram; (d) enlarged histogram from (c) showing the details in the short spacing range from 0 to 200 nm. The sharp high frequency peak at 3.1 nm in (d) is an indication of the intercalation. Curve fitting by lognormal distribution is superimposed and the arrowheads indicate the mean spacing position.

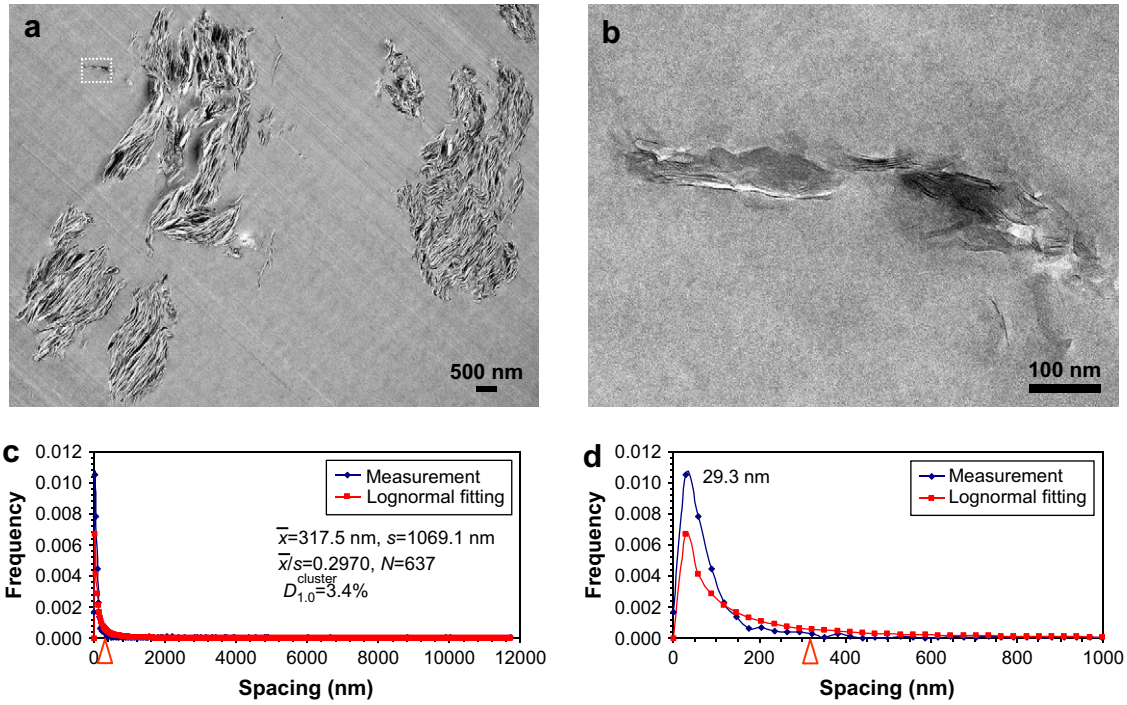

Fig. 7. (a) Low-magnification image of immiscible PT15 with 5 wt% 30B taken at larger defocus; (b) high-magnification image taken at near Scherzer defocus, from the framed area in (a) showing the single sheet is indeed a cluster of individual platelets; (c) spacing histogram measured from the cluster sheets in (a); (d) enlarged histogram from (c) showing the details in the short spacing range from 0 to 1000 nm. Curve fitting by lognormal distribution is superimposed and the arrowhead indicates the mean spacing position.

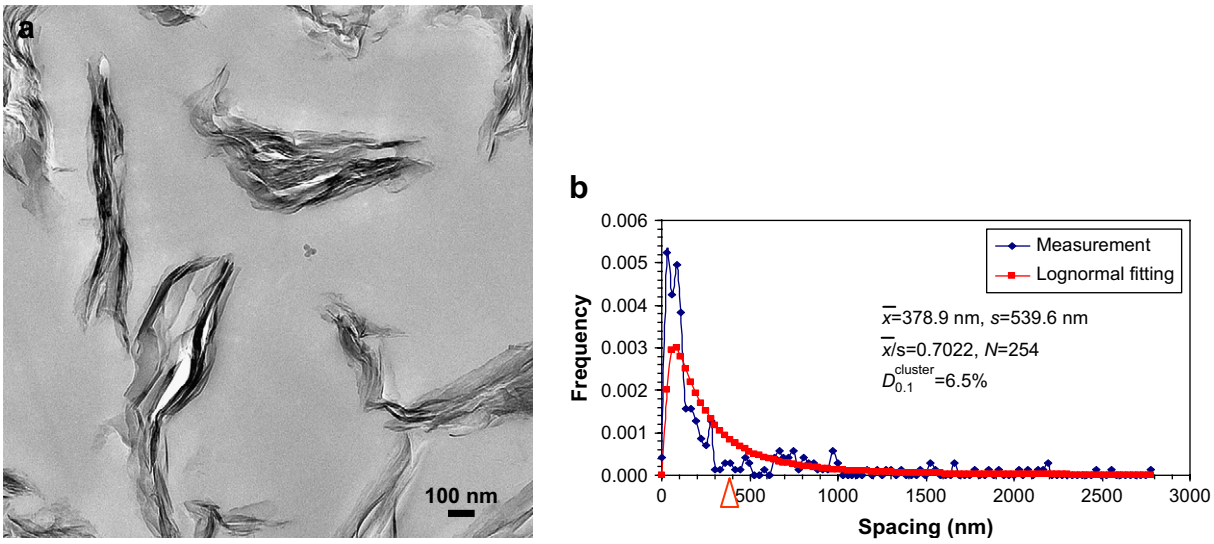

Fig. 8. (a) Microstructure of immiscible epoxy with 2 wt% 30B; (b) cluster spacing histogram measured from (a). Curve fitting by lognormal distribution is superimposed and the arrowhead indicates the mean spacing position.

5 wt% 30B clay. The 1230 FR particles appear as well-dispersed dark dots. In the magnified image in Fig. 9(b) from the framed area in (a), the clay layers are visible. They are seen as exfoliated but also intercalated for some part of the layers. Fig. 9(a) is divided by 20×20 grid lines along the horizontal and vertical directions, respectively, and the spacing between the 1230 FR particles are measured to construct the histogram as shown in (c). The mean spacing of the 1230 FR particles is measured as 1235.4 nm, with a standard deviation of 1018.5 nm, $\bar{x}/s = 1.2130$, hence $D_{0.1} = 10.4\%$. On the other hand, the histogram of the clay filler, from Fig. 9(b) by 20×20 grid lines, is constructed in (d). The mean spacing of the clay platelets is measured as 55.0 nm, with a standard deviation of 61.2 nm, $\bar{x}/s = 0.8987$, hence $D_{0.1} = 8.0\%$ for 30B. As the PA11 samples with only 30B have similar dispersion levels (Table 1), the addition of the 1230 FR particles does not affect the dispersion level of the clay particles. It is noted that a peak at 4.1 nm

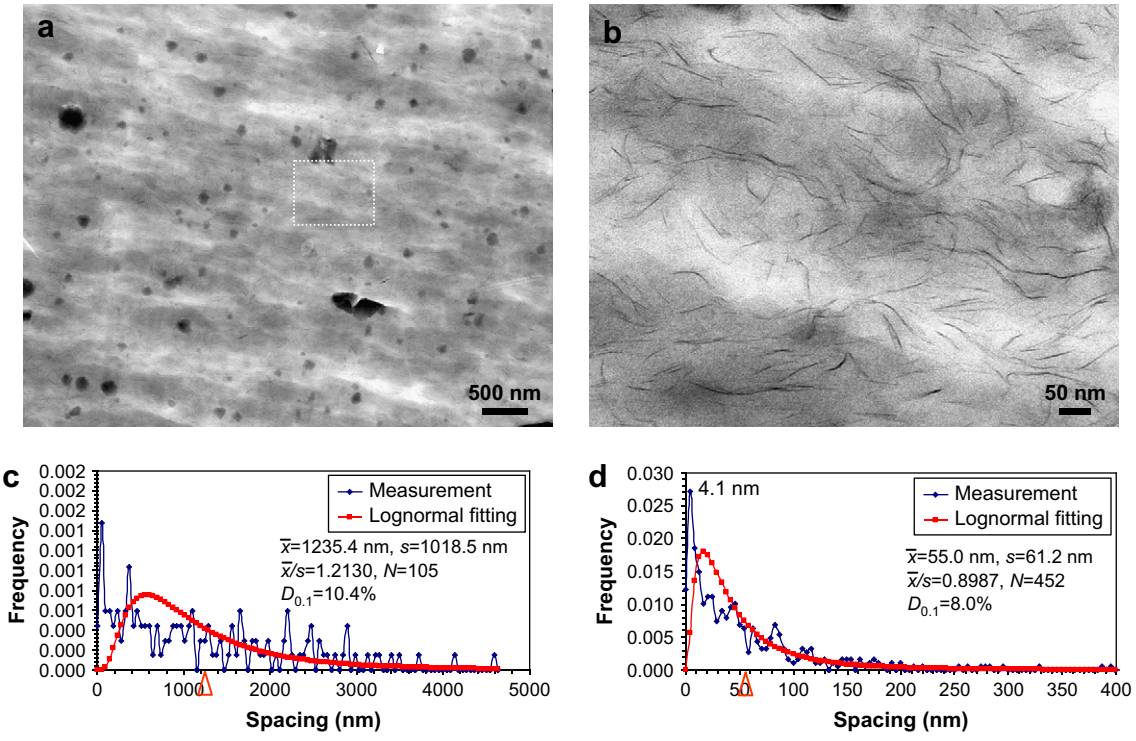

Fig. 9. Microstructure and dispersion quantification with two fillers, PA11 with 20 wt% 1230 FR particles and 5 wt% 30B clay. (a) Low-magnification image, where the 1230 FR particles exhibit dark contrast; (b) high-magnification image from the framed area in (a) showing clay layers; (c) spacing histogram of the 1230 FR particles measured from (a); (d) spacing histogram of the clay layers measured from (b). Curve fittings by lognormal distribution are superimposed, and the arrowheads indicate the mean spacing positions.

appears in Fig. 9(d), although it is not as high as those seen in Figs. 5 and 6 for the intercalation case. This peak indicates that this sample is probably at the middle between exfoliation and intercalation. Therefore, it may be reasonable to suggest the dispersion above 8% as exfoliated, and below it, as intercalated.

Fig. 10 shows a microstructure of PA11 with 20 wt% 1230 FR particles but with a higher level of 7.5 wt% 30B clay. The clay platelets are exfoliated and well dispersed along with the 1230 FR particles. The image is divided by 10 × 10 grid lines, and the constructed histogram based on the spacing distance measurement is shown in Fig. 10(b). The mean spacing of the clay platelets is measured as 40.4 nm, with a standard deviation of 42.3 nm, $\bar{x}/s = 0.9551$, hence $D_{0.1} = 8.5\%$. It belongs to the exfoliated type.

4. Discussion

4.1. Distinguishing exfoliation and intercalation

As pointed out by Utracki [47], for completely exfoliated PLSNs with disordered structure, the clay volume fraction ϕ satisfies:

$$\phi < \phi_{\max}; \tag{2a}$$

whereas for ordered structure,

$$\phi > \phi_{\max}. \tag{2b}$$

Here $\phi_{\max}$ is the maximum volume fraction, which is given by:

$$\phi_{\max} = 0.93/p, \tag{3}$$

where p is the aspect ratio. For the 30B clay, if one takes $p = 300$, $\phi_{\max} = 0.31\%$.

In the present samples, the specific gravity of 30B clay is 1.9–2.1 g/cc according to the manufacture's data sheet, so we take $\rho_{30B} = 2$ g/cc. The PA11 polymer matrix has specific gravity of 1.04 g/cc, hence we assume $\rho_{\text{matrix}} = 1.04$ g/cc. The 0.31% volume fraction converts to 0.59% weight percent, which is much lower than the clay content used in this work. The exfoliated structures observed, as shown in Figs. 3 and 4, in fact contain certain local ordering, although the entire structure at a larger scale is disordered, and there are some stacks containing few platelets. However, the majority of the clay platelets are separated as single isolated layers, so we still define this case as exfoliated structure. In the case of intercalation, most of the agglomerates contain a certain number of platelets, although their internal spacing may increase from their original spacing d_0. In this case, a sharp high frequency peak appears at a short spacing distance in the histogram (Figs. 5d and 6d), which is a clear characteristic indication for the intercalation. The histogram is a good tool to distinguish the exfoliation and intercalation. According to this work, exfoliation structure typically has $D_{0.1}$ higher than 8%, while the intercalated structure has $D_{0.1}$ typically between 4 and 8%.

4.2. Comparison of this method to previous methods

It is necessary to compare the method presented in this work with previous methodologies to get a better understanding. As mentioned in Section 1, previous work developed dispersion evaluations using TEM by: (1) PSM [26,30], (2) PDM [25,27], and (3) LIDM [29]. As shown in Fig. 11(a), the PSM is very useful for intercalated or immiscible system with large evident tactoids, since dispersion can be evaluated from the size of tactoids by the parameters of the clay particle length L_{clay}, clay particle thickness d_{clay}, correlation length ξ_{clay}, and particle aspect ratio AR. However, when the system becomes exfoliated, these parameters become constants for single platelets.

The PDM is universally applicable to exfoliated, intercalated or immiscible system. It is especially useful for systems containing stacks with different size at the same loading level, because the density is related to the clay loading. However, this method does not count the internal spacing between the clay particles. An example is shown in Fig. 11(b) and (c), both of them have exactly the same number of particles but

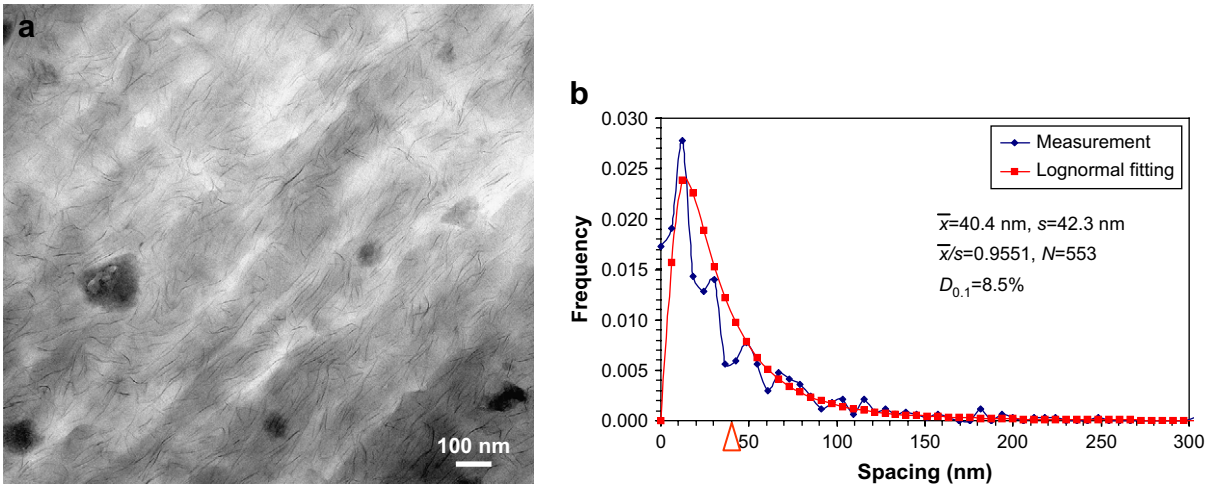

Fig. 10. (a) Microstructure of PA11 with 20 wt% 1230 FR particles and 7.5 wt% 30B clay taken at larger defocus; (b) spacing histogram of the clay layers. Curve fitting by lognormal distribution is superimposed, and the arrowhead indicates the mean spacing position.

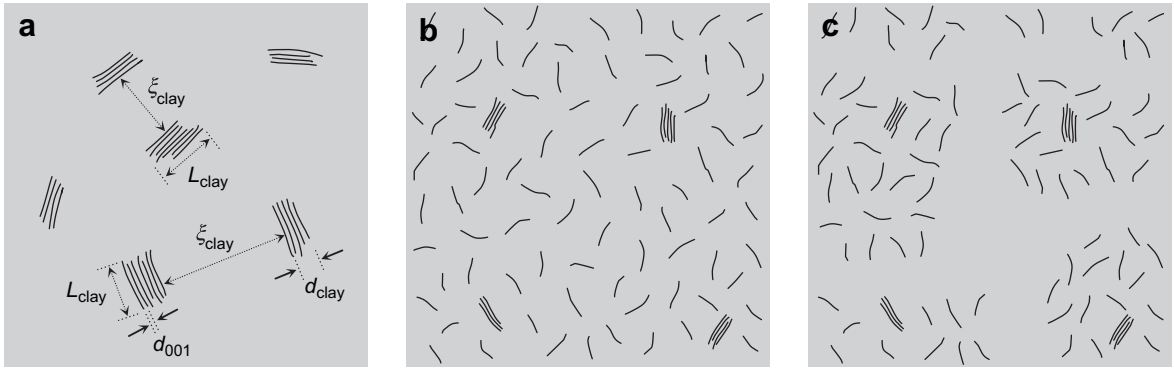

Fig. 11. Schematic microstructure. (a) Intercalated structure to show the particle size measurements; (b) well-dispersed exfoliated/intercalated structure; (c) less dispersion as compared to (b).

with different dispersion. The density counting would produce the same results for them.

The LIDM monitors the dispersion from the intercept spacing between the clay stacks along the intercept lines. A comparison of LIDM with PSM and PDM was given previously [29]. However, the distance given by the LIDM is related to the clay loading level.

For the method presented in this work, FPSM, its starting point is indeed similar to the LIDM, as both of them use array of parallel lines to intercept the clay particles for the distance measurement. However, there are several differences: (1) the LIDM measures the spacing between stacks (otherwise, if ones counts single layers between within stacks, the intercept distance would be the same for a given system with the same loading), while FPSM measures the free-path spacing between the single layer sheets; (2) the LIDM is dependent to the loading, while the FPSM only deals with the free-path spacing data distribution, and thus $D_{0.1}$ is independent to the loading and it is dimensionless.

The FPSM is mainly designed for exfoliated and intercalated microstructures with small size tactoids. For the exfoliated or intercalated structures like that shown in Fig. 11 (b) and (c), the FPSM method could distinguish their dispersion degrees, because it is based upon their spacing measurement. However, as demonstrated previously, for a system containing larger tactoids, this method works difficultly because it is hard to count the spacing within the large tactoids. Although trials have been made using larger defocus to image clusters, as demonstrated in Figs. 7 and 8, the cluster dispersion is not comparable to the single sheet dispersion, and the appearance of the clusters depends on the defocus values applied in some samples. However, a future extension of this work may involve a lower resolution tool, like scanning electron microscopy (SEM) or optical microscopy (OM), to image these large tactoids and apply the same methodology to quantify their dispersion parameter $D_{0.1}$.

4.3. Layer spacing of exfoliated/intercalated samples

The FPSM method gives mean free-path spacing data of the single layers, as listed in Table 1. If one ignores the layer thickness that is about 1 nm, this spacing is the mean layer spacing d, i.e. $d \approx x$. When a line intercepts the clay sheets, the mean line fraction $L_L = d_0/d$. Here note that the effective thickness of each sheet is d_0, as the clay volume fraction is based on the volume of the original clay particles with d_0 spacing between the sheets. According to the stereological principle, L_L equals the volume faction V_V, or ϕ:

$$\phi = d_0/d, \tag{4}$$

and hence

$$d = d_0/\phi. \tag{5}$$

According to this relationship, when $\phi \to 0$, $d \to \infty$ and when $\phi = 1$, $d = d_0$, which is the original clay layer spacing (layers completely attached, with a spacing of d_0). Eckel et al. [29] used this equation to estimate the intercept distance of their samples. Taking $d_0 = 1.85$ nm to convert the volume fraction into weight fraction as follows:

$$d = \frac{1.85}{\phi} = 1.85\frac{w/\rho_{30B} + (1-w)/\rho_{matrix}}{w/\rho_{30B}} = -1.707 + 3.558/w. \tag{6}$$

For the weight percent content studied in this work, if one supposes that the polymer matrices have the same specific gravity, $\rho_{matrix} = 1.04$ g/cc, as used in the above equation, the theoretical layer spacing can be calculated using Eq. (6), as plotted in Fig. 12. The measured spacing data are close to the calculated ones, as listed in Table 2. The relationship between measured d and w is expressed as the following function by regression of the experimental data:

$$d = 6.936 + 2.590/w, \tag{7}$$

with correlation coefficient $R = 0.990$.

Here, we also compare d with d_{001}, which is the basal layer spacing of stacks. Utracki [47] reduced a relationship between d_{001} and w as follows:

$$d_{001} = a_0 + a_1/w, \tag{8}$$

where a_0 and a_1 are two fitting parameters. Using the d_{001} data determined by Okada and Usuki [48], Utracki [47] gives:

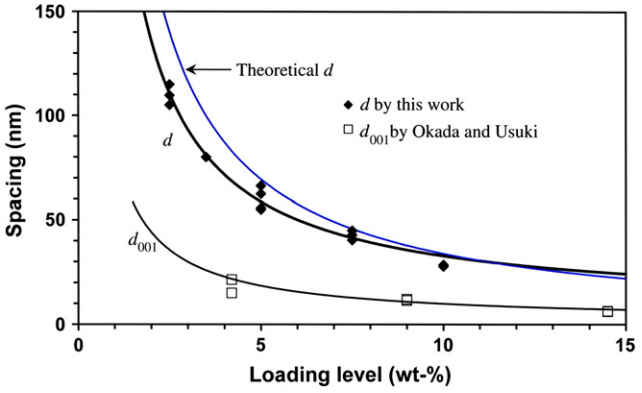

Fig. 12. Clay layer spacing (nm) as a function of the loading level (wt%).

Table 2
Comparison of measured and theoretical layer spacing (nm)

Loading level (wt%)	Measured spacing (nm)	Theoretical spacing (nm)
2.5	105.1, 109.7, 115, 107.5	140.6
3.5	80.0	100.0
5.0	66.3, 55.8, 62.5, 55.0	69.5
7.5	45.0, 42.9, 44.9, 40.4	45.7
10.0	27.8, 28.6	33.9

$$d_{001} = 1.37 + 0.865/w, \tag{9}$$

with correlation coefficient $R = 0.991$. The d_{001} is also plotted in Fig. 12 for comparison. It is seem that both d and d_{001} have the same inversely proportional relationship to w. As d is measured from the single layer spacing, while d_{001} is measured from layers within the stacks only (usually by XRD), d is always greater than d_{001}, while they are getting closer at higher loading levels.

5. Summary of this work

In this work, we present a new TEM methodology to quantify the clay dispersion in clay/polymer nanocomposites. This method, named as free-path spacing measurement, is based on the measurement of the free-path spacing distance between the single clay sheets. The dispersion value $D_{0.1}$ is calculated from the distribution of the free-path spacing data according to Eq. (1). The $D_{0.1}$ parameter is dimensionless and is not related to the filler size, shape, aggregation, concentration, or the existence of additional filler.

Several examples of exfoliated, intercalated, and immiscible samples were studied. It was found that exfoliated composites had $D_{0.1}$ over 8%, while the intercalated composites have 4–8%. In the case of intercalation, a high frequency peak appears at a short spacing distance in the histogram, which is an evident characteristic indication for the intercalation. This main utility of this methodology is for exfoliated or intercalated samples but with small number of layers with the stacks.

The dispersion below 4% was suggested to classify as immiscible. In the immiscible case, it is difficult to use the TEM method to quantify the dispersion level $D_{0.1}$, which is the weakness of this methodology. A trial was made using the layer clusters, which were imaged at larger defocus values.

The unique advantage of the TEM measurement is that the dispersion degrees of different fillers can be measured individually, because the different fillers can be visually differentiated or chemically identified in TEM via EDS or EELS. It was demonstrated that the addition of the 1230 FR particles into the PA11 matrix did not affect the dispersion level of the 30B clay, and the dispersion levels of both 1230 FR and 30B fillers were quantified individually.

Acknowledgements

This work was supported by the Air Force Office of Scientific Research (AFOSR), Arlington, VA. The authors thank Rick Littleton for technical assistance in the TEM sample preparation, and Dr. Andreas Holzenburg for his encouragements to this research. Critical comments from the previous reviewers are especially appreciated for improving this paper.

References

[1] Carter LW, Hendricks JG, Bolley DS. Elastomer reinforced with a modified clay. U.S. Patent no. 2531; 1950. p. 396–400.
[2] Ray SS, Okamoto M. Prog Polym Sci 2003;28(11):1539–641.
[3] Morgan AB, Gilman JW. J Appl Polym Sci 2003;87(8):1329–38.
[4] Kojima Y, Usuki A, Kawasumi M, Okada A, Fukushima Y, Kurauchi T, et al. J Mater Res 1993;8(5):1185–9.
[5] Gilman JW, Jackson CL, Morgan AB, Harris R, Manias E, Giannelis EP, et al. Chem Mater 2000;12(7):1866–73.
[6] Zhu J, Morgan AB, Lamelas FJ, Wilkie CA. Chem Mater 2001;13(10):3774–80.
[7] Krikorian V, Pochan DJ. Chem Mater 2003;15(22):4317–24.
[8] Gurmendi U, Eguiazabal JI, Nazabal J. Compos Sci Technol 2006;66(10):1221–8.
[9] Usuki A, Kojima Y, Kawasumi M, Okada A, Fukushima Y, Kurauchi T, et al. J Mater Res 1993;8(5):1179–84.
[10] Weimer MW, Chen H, Giannelis EP, Sogah DY. J Am Chem Soc 1999;121(7):1615–6.
[11] Zeng CC, Lee LJ. Macromolecules 2001;34(12):4098–103.
[12] Zeng QH, Wang DZ, Yu AB, Lu GQ. Nanotechnology 2002;13(5):549–53.
[13] Uthirakumar P, Nahm KS, Hahn YB, Lee YS. Eur Polym J 2004;40(11):2437–44.
[14] Ray S, Galgali G, Lele A, Sivaram S. J Polym Sci Part A Polym Chem 2005;43(2):304–18.
[15] Vaia RA, Ishii H, Giannelis EP. Chem Mater 1993;5(12):1694–6.
[16] Liu LM, Qi ZN, Zhu XG. J Appl Polym Sci 1999;71(7):1133–8.
[17] Cho JW, Paul DR. Polymer 2001;42(3):1083–94.
[18] Yoon JT, Jo WH, Lee MS, Ko MB. Polymer 2001;42(1):329–36.
[19] Wang SF, Hu Y, Wang ZZ, Yong T, Chen ZY, Fan WC. Polym Degrad Stab 2003;80(1):157–61.
[20] Mohanty S, Nayak SK. Polym Compos 2007;28(2):153–62.
[21] Guo BC, Jia DM, Cai CG. Eur Polym J 2004;40(8):1743–8.
[22] Liu TX, Tjiu WWC, He CB, Na SS, Chung TS. Polym Int 2004;53(4):392–9.
[23] Vaia RA, Jandt KD, Kramer EJ, Giannelis EP. Chem Mater 1996;8(11):2628–35.
[24] Kornmann X, Lindberg H, Berglund LA. Polymer 2001;42(4):1303–10.
[25] Dennis HR, Hunter DL, Chang D, Kim S, White JL, Cho JW, et al. Polymer 2001;42(23):9513–22.
[26] Nam PH, Maiti P, Okamoto M, Kotaka T, Hasegawa N, Usuki A. Polymer 2001;42(23):9633–40.

[27] Fornes TD, Yoon PJ, Keskkula H, Paul DR. Polymer 2001;42(25): 9929–40.
[28] Lee SR, Park HM, Lim H, Kang TY, Li XC, Cho WJ, et al. Polymer 2002;43(8):2495–500.
[29] Eckel DF, Balogh MP, Fasulo PD, Rodgers WR. J Appl Polym Sci 2004;93(3):1110–7.
[30] Vermogen A, Masenelli-Varlot K, Seguela R, Duchet-Rumeau J, Boucard S, Prele P. Macromolecules 2005;38(23):9661–9.
[31] Bourbigot S, Vanderhart DL, Gilman JW, Bellayer S, Stretz H, Paul DR. Polymer 2004;45(22):7627–38.
[32] Bertmer M, Wang MF, Krüger M, Blümich B, Litvinov VM, van Es M. Chem Mater 2007;19(5):1089–97.
[33] Zhao J, Morgan AB, Harris JD. Polymer 2005;46(20):8641–60.
[34] Zilg C, Mulhaupt R, Finter J. Macromol Chem Phys 1999;200(3): 661–70.
[35] Chin IJ, Thurn-Albrecht T, Kim HC, Russell TP, Wang J. Polymer 2001;42(13):5947–52.
[36] Underwood EE. Quantitative stereology. Reading: Addison-Wesley; 1970.
[37] Moore GA. Recent progress in automatic image analysis. J Microsc 1972;95(2):105–18.
[38] Russ JC. Practical stereology. New York: Plenum Press; 1986.
[39] Howard CV, Reed MG. Unbiased stereology: three-dimensional measurement in microscopy. Oxford: BIOS Scientific Publishers Limited; 1998.
[40] Higginson RL, Sellars CM. Worked examples in quantitative metallography. London: Maney; 2003.
[41] Williams DB, Carter CB. Transmission electron microscopy: a textbook for materials science. New York: Plenum Press; 1996. p. 466.
[42] Luo ZP. Acta Mater 2006;54(1):47–58.
[43] Luo ZP, Koo JH. J Microsc 2007;225(2):118–25.
[44] Abramoff MD, Magelhaes PJ, Ram SJ. Biophotonics Int 2004;11(7):36–42.
[45] Fornes TD, Paul DR. Macromolecules 2004;37(20):7698–709.
[46] McNally T, Murphy WR, Lew CY, Turner RJ, Brennan GP. Polymer 2003;44(9):2761–72.
[47] Utracki LA. Clay-containing polymeric nanocomposites. Shawbury, United Kingdom: Rapra Technology Limited; 2004. p. 201–205.
[48] Okada A, Usuki A. Mater Sci Eng C 1995;3(2):109–15.